geoconvention
Virtual Event
September 13 - 15
2021

Simultaneous inversion for anisotropy parameters and microseismic-event locations in orthorhombic media

Hongliang Zhang, Jan Dettmer, Joe Wong and Kristopher A. Innanen
Department of Geoscience, University of Calgary

Summary

To account for anisotropy caused by the presence of a set of aligned vertical fractures in a finely horizontally layered background medium, we present a Bayesian inversion procedure to simultaneously estimate microseismic event locations and anisotropy parameters for orthorhombic (ORT) media. To ensure efficient sampling of the parameter space, the Bayesian inference is employed via Markov-chain Monte Carlo (McMC) sampling with parallel tempering and principal component diminishing adaptation. The uncertainty is quantified by approximating the posterior probability density with an ensemble of model-parameter sets. For the ORT media, the quasi-P-wave group velocities are approximated by linearization. The proposed inversion algorithm is exemplified through an application to a physical modelling dataset, in which the ORT medium is approximately represented by a phenolic CE material.

Method

In ORT media, the density-normalized stiffness matrix **A** can be represented as

$$\mathbf{A} = \begin{bmatrix} A_{11} & A_{12} & A_{13} & & & \\ A_{12} & A_{22} & A_{23} & & & \\ A_{13} & A_{23} & A_{33} & & & \\ & & & A_{44} & & \\ & & & & A_{55} & \\ & & & & & A_{66} \end{bmatrix}. \tag{1}$$

where the A_{ii} (i = 1, 2, 3) are related to the qP-wave velocities V_{11}, V_{22}, and V_{33} along x_1, x_2, and x_3 axes, respectively. These velocities are given by $A_{ii} = V_{ii}^2$. The A_{ii} (i = 4, 5, 6) are related to qS-wave velocities, given by $A_{44} = V_{23}^2 = V_{32}^2$, $A_{55} = V_{13}^2 = V_{31}^2$ and $A_{66} = V_{12}^2 = V_{21}^2$. According to Daley and Krebes (2016), the qP-wave group velocity in ORT media can be approximated by linearization as

$$\frac{1}{V_P^2(\mathbf{N})} = \frac{N_1^2}{A_{11}} + \frac{N_2^2}{A_{22}} + \frac{N_3^2}{A_{33}} - \frac{E_{12}N_1^2N_2^2}{A_{11}A_{22}} - \frac{E_{13}N_1^2N_3^2}{A_{11}A_{33}} - \frac{E_{23}N_2^2N_3^2}{A_{22}A_{33}}, \tag{2}$$

where **N** is the unit vector in the ray direction that can be represented in polar coordinates. The E_{ij} (ij = 12, 13, 23) are defined as

$$E_{12} = 2(A_{12} + 2A_{66}) - (A_{11} + A_{22}), \tag{3}$$

$$E_{13} = 2(A_{13} + 2A_{55}) - (A_{11} + A_{33}), \tag{4}$$

and

$$E_{23} = 2(A_{23} + 2A_{44}) - (A_{22} + A_{33}). \tag{5}$$

In this study, since the inversion is based on P-wave first arrivals only, it is not possible to resolve all nine stiffness coefficients, especially those related to qS-wave velocities (A_{44}, A_{55}, A_{66}). To reduce parametrization complexity, here we define three parameters B_1 = 2(A_{12}+2A_{66}), B_2 = 2(A_{13}+2A_{55}), and B_3 = 2(A_{23}+2A_{44}). Then, the qP-wave group velocity along any ray direction can be obtained from eq. (2) using the modified parameterization with six independent parameters (V_{11}, V_{22}, V_{33}, B_1, B_2, B_3).

According to Bayes' theorem, the posterior probability density is expressed as

$$P(\mathbf{m}\,|\,\mathbf{d}) \propto P(\mathbf{d}\,|\,\mathbf{m})P(\mathbf{m}), \tag{6}$$

where **m** and **d** are model and data vectors, respectively, and $P(\mathbf{d}|\mathbf{m})$ is the likelihood function. The prior probability is given by $P(\mathbf{m})$. Under the assumption of independent and identically distributed Gaussian noise, the likelihood function is

$$P(\mathbf{d}\,|\,\mathbf{m}) = \frac{1}{(2\pi)^{N/2}\sigma_d^N} \exp\left[-(\mathbf{d} - g(\mathbf{m}))^T(\mathbf{d} - g(\mathbf{m}))/(2\sigma_d^2)\right], \tag{7}$$

where σ_d is the noise standard deviation, g is the forward model and N is the number of observed data.

In microseismic data processing, perforation shots are usually used to calibration the velocity model, and locations of perforation shots are generally not known accurately due to measurement errors. Therefore, we treat these locations as unknown but assign narrow distributions around the recorded perforation-shot locations as priors to reflect reasonable location uncertainty. For microseismic events, we assign broad uniform priors for hypocenter location (x, y, z). Origin times (t_0) for perforation shots and microseismic events are generally poorly known or unknown and are included as unknown in the inversion. In addition, orientations three mutually orthogonal planes of ORT media are also unknown. Therefore, we include an additional unknown in the inversion. Here, we define x_1, x_2 and x_3 as the three axes that are perpendicular to the three mutually orthogonal planes, and this unknown is the angle (θ) between the x_1 axis and the x axis in the coordinate system used for data acquisition. Thus, for the simultaneous inversion problem, **m** is $[\,\theta, V_{11}, V_{22}, V_{33}, B_1, B_2, B_3, t_0^{(1)}, x_0^{(1)}, y_0^{(1)}, z_0^{(1)}, \cdots, t_0^{(K)}, x_0^{(K)}, y_0^{(K)}, z_0^{(K)}, \sigma_d\,]$, where K is the total number of events. In the inversion, the model parameters can be estimated by McMC sampling. To improve the sampling efficiency, we adopt parallel tempering (Earl and Deem 2005; Dettmer and Dosso 2012) that permits probabilistic exchange of model vectors between Markov-chains with different tempering parameters. In addition, to overcome the inefficiency due to correlated parameters, we

adopt a proposal distribution along principal axes (Dosso *et al.,* 2014). The proposal distribution is considered as a univariate Cauchy distribution along principal axes of the parameter space.

Physical Modeling Data

To demonstrate the effectiveness of the proposed inversion algorithm, we apply it to a physical modeling data. The experiment is a miniaturized version of the filed monitoring with a model scale factor 1:10,000 for both time and space domains. In the physical modeling experiment, we use a phenolic CE laminate material to mimic the ORT medium. Figure 1 shows the acquisition geometry, in which a simulated star-shaped surface-receiver array is used. Eight perforation shots are available and 11 microseismic events have unknown locations to be determined through the inversion. Due to practical constraints for the placement of transducers near and within solid targets, the phenolic slab is immersed in a water tank, and sources and receivers are placed in water.

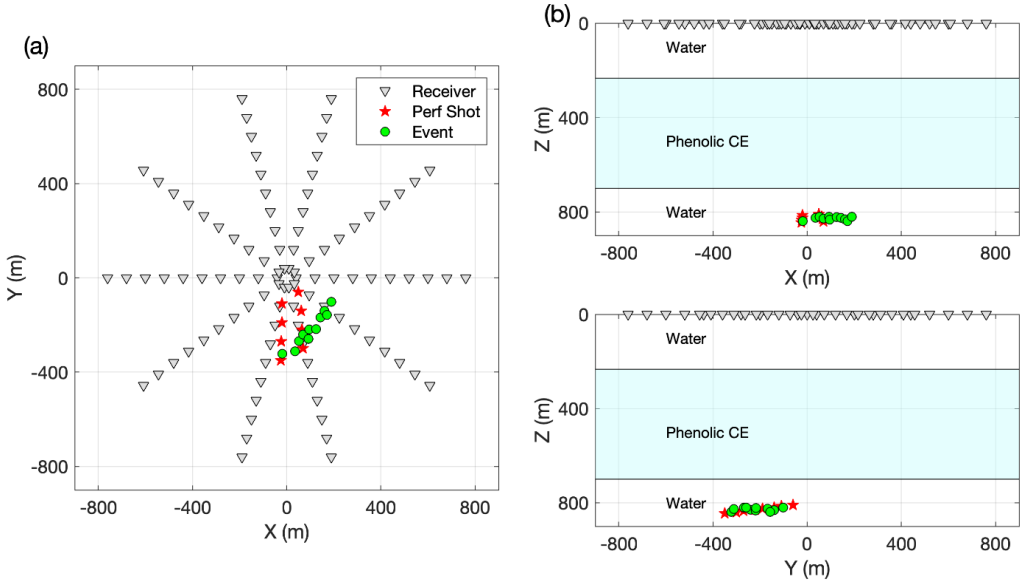

Figure 1 Map view (a) and side views (b) of the acquisition geometry for the physical modelling experiment.

Results

The Bayesian inversions is performed for laboratory data with the ORT-model approximation for the phenolic block. Since origin times are known at time zero for the experiment, we apply simultaneous inversion with known origin times for both perforation shots and microseismic events. Figure 2 presents the posterior marginal distributions for anisotropy parameters, θ and noise standard deviation, which appear Gaussian-like. At the stage of setting up the acquisition geometry, the ORT x_1 axis was placed at approximately 90° from the x axis of the acquisition coordinates. The θ value is very close to this value, with mode of posterior marginal at ~88.8°. Three velocities are estimated in the inversion, i.e., V_{11}, V_{22}, V_{33}. Most velocity estimates have narrow uncertainties, less than 50 m/s in terms of 95% credibility intervals. However, the uncertainty for V_{22} is broader. Estimated noise standard deviation exhibits mode of posterior marginal at 1.3 ms.

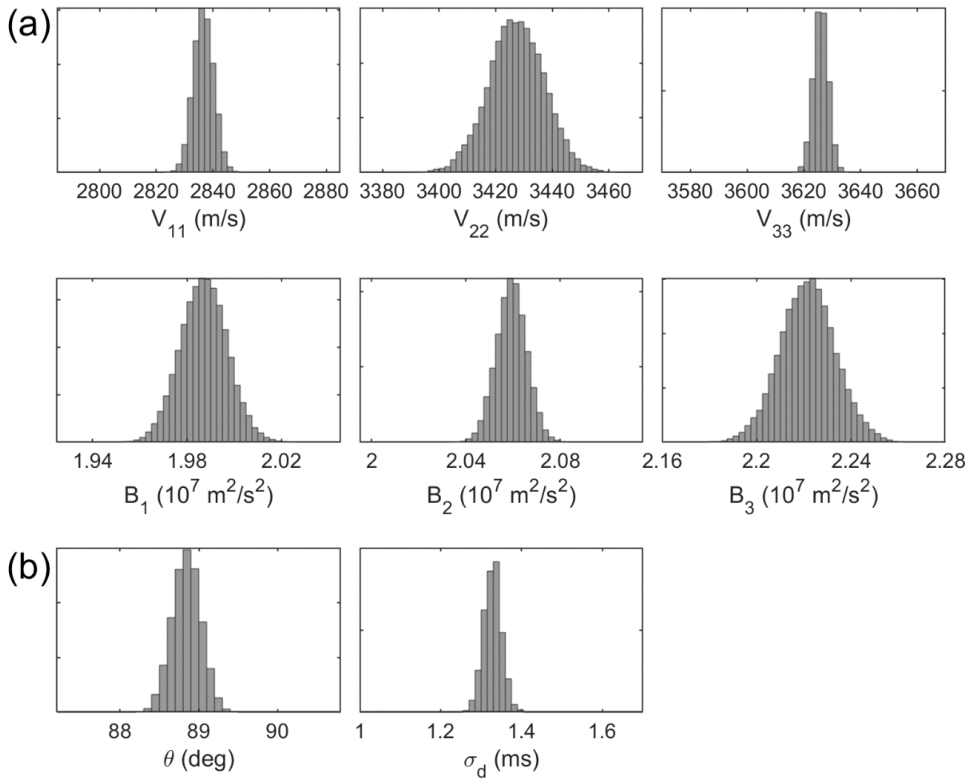

Figure 2 Marginal distributions for estimated (a) anisotropy parameters and (b) deviation angles (θ) of symmetry axis and x_1 axis from the x axis in the coordinate system as well as the noise standard deviation (σ_d).

Figure 3 presents epicenter marginals for eight perforation shots and 11 microseismic events. The 95% CIs average 4.6 m and 4.5 m along the x and y directions, respectively. Figure 3 also shows event positions recorded during the experiment. A systematic shift can be observed between inversion estimates and recorded positions especially along y direction. The shift is on average 11.8 m in y direction. The systematic shifts are easier to be observed in the marginal distributions of residuals in hypocenters in Figure 4. These shifts are caused mainly by errors in setting the origins of the receiver and source coordinate systems. The source and receiver transducers are moved independently by separate electric motors, so the origins of the source and receiver coordinate systems must be aligned manually and visually. Because the diameters of the transducers are 2.36mm in size (23.6m in scaled survey coordinates), misalignments of the origin positions by as much as 1.20mm (12.0m in scaled survey coordinates) in both x and y are quite possible. In terms of marginal distributions of residuals in event depths shown in Figure 4, the ORT model estimates depths to be slightly deeper than the recorded values. This systematic deviation is also likely caused by the measurement error due to the piezoelectric-pin size. Since all the shifts caused by origin misalignment are systematic, they could have been eliminated just by applying constant corrections to the receiver coordinates.

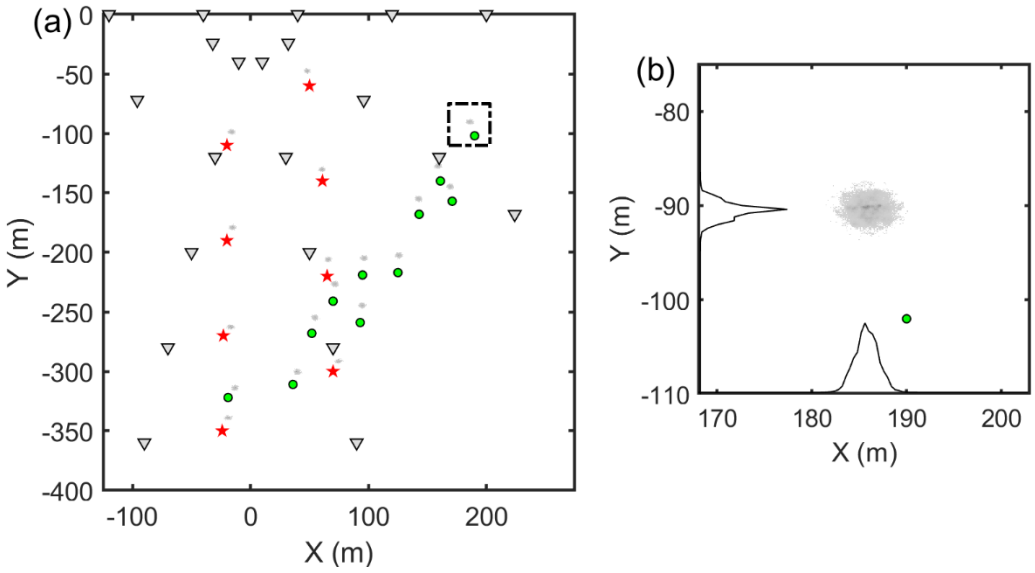

Figure 3 (a) Epicenter marginal distributions. (b) An enlargement of the dashed box in (a) with 1D marginals along the *x* and *y* axes.

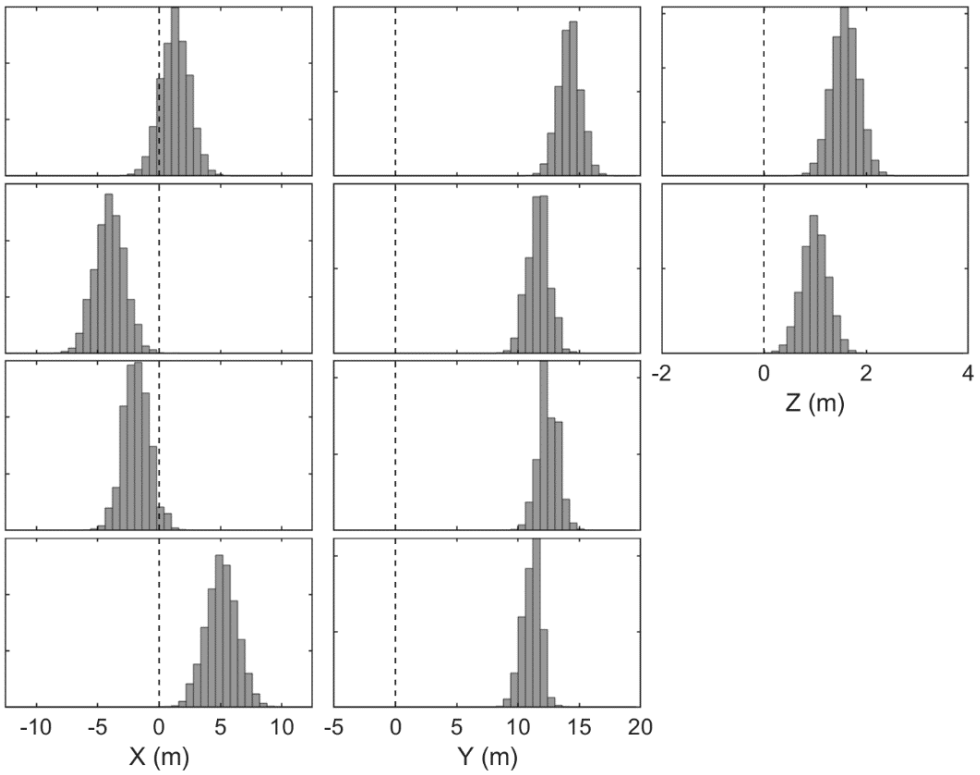

Figure 4 Marginals of absolute errors in hypocenters for two typical microseismic events (the first two rows) and epicenters for two typical perforation shots (the last two rows).

Conclusions

We have presented a probabilistic approach to simultaneously estimate microseismic event locations and anisotropy parameters in ORT media. The inversion rigorously quantifies parameter uncertainties by treating locations for microseismic events, horizontal locations of perforation shots, effective anisotropy parameters, and the noise standard deviation as unknown. The simultaneous inversion approach has been applied to a physical modelling dataset, in which a phenolic CE layer is approximately considered as an ORT medium. This physical modeling study demonstrates that the inversion can account for measurement errors within the recorded perforation-shot locations by assigning them priors with narrow ranges, and the proposed algorithm can place them into more reliable locations. In future research, we will consider the inclusion of additional event time constraints so that unknown origin times can be estimated by the inversion.

Acknowledgements

This work was funded by the industrial sponsors of the Consortium for Research in Elastic Wave Exploration Seismology (CREWES), by the NSERC grants CRDPJ 461179-13 and CRDPJ 543578-19, and also in part by the Canada First Research Excellence Fund. We are grateful for the help from Kevin Bertram to set up physical models.

References

Daley, P. F. and Krebes, E. S., 2016. A linearized group velocity approach for two-point qP ray tracing in a layered orthorhombic medium, *J. Seism. Explor*., **25**(1), 87-101.

Dettmer, J. and Dosso, S. E., 2012. Trans-dimensional matched-field geoacoustic inversion with hierarchical error models and interacting Markov chains, *J. Acoust. Soc. Am*., **132**(4), 2239-2250.

Dosso, S. E., Dettmer, J., Steininger, G. and Holland, C. W., 2014. Efficient trans-dimensional Bayesian inversion for geoacoustic profile estimation, *Inverse Probl*., **30**(11), 114018.

Earl, D. J. and Deem, M. W., 2005. Parallel tempering: Theory, application, and new perspectives, *Phys. Chem. Chem. Phys*., **7**(23), 3910-3916.